Desalination and Water Treatment
www.deswater.com

doi: 10.1080/19443994.2015.1021102

57 (2016) 58–74
January

Taylor & Francis
Taylor & Francis Group

An off-grid stand-alone wave energy supply system with maximum power extraction scheme for green energy utilization in Malaysian Island

Nahidul Hoque Samrat[a], Norhafizan Ahmad[a,*], Imtiaz Ahmed Choudhury[a], Zahari Taha[b]

[a]*Faculty of Engineering, Department of Mechanical Engineering, Centre for Product Design and Manufacturing (CPDM), University of Malaya, 50603 Kuala Lumpur, Malaysia, email: sam_3e60@yahoo.com (N.H. Samrat), Tel. +60 3 79677625; Fax: +60 3 79675317; emails: norhafizan@um.edu.my (N. Ahmad), imtiaz@um.edu.my (I.A. Choudhury)*
[b]*Faculty of Manufacturing Engineering, Innovative Manufacturing, Mechatronics and Sports Laboratory (iMAMS), University Malaysia Pahang, 26600 Pekan, Pahang, Malaysia, email: zaharitaha@ump.edu.my*

Received 5 October 2014; Accepted 16 November 2014

ABSTRACT

Energy is one of the most important factors in the socioeconomic development of a country. In a developing country like Malaysia, the development of islands is mostly related to the availability of electric power. As an island surrounded by sea, power generated by wave energy source will become one of the most promising solutions for the electrification of island areas. But, the unpredictable nature of the wave energy source is the main drawback. This paper presents a novel stand-alone wave energy supply system modeling with maximum power tracking and an energy storage-based power management algorithm in MATLAB/Simulink environment. The main contributions of this research work are eliminating the intermittent power generation nature of wave energy and efficiently extract the maximum wave power. In the proposed stand-alone system, a DC–DC bidirectional buck-boost converter controller is used to maintain the constant dc-link voltage. It also accumulates the surplus wave power in the battery bank and supplies this power to the load during the wave power shortage. A three-phase complex vector control scheme voltage source inverter is used to control the load-side voltage in terms of the frequency and voltage amplitude. Based on the simulation results obtained from MATLAB/Simulink, it has been found that the overall system is capable of working under variable weather and load conditions, and it can also able to extract the maximum wave power.

Keywords: Stand-alone system; Oscillating water column (OWC); Maximum power point tracking (MPPT); Island; Battery bank; Simulation; Dc-link voltage

*Corresponding author.

Presented at the International Conference on Business, Economics, Energy and Environmental Sciences (ICBEEES) 19–21 September 2014, Kuala Lumpur, Malaysia

1. Introduction

Energy was, is, and will remain one of the fundamental economic development foundations of any nation. The majority of the island development problems all over Malaysia are mostly related to energy production. Most of the offshore islands in Malaysia use fossil fuels to generate electricity even though Malaysia has a good mix of renewable energy sources such as solar, wind, wave, biomass, and hydro. The energy produced by the traditional sources increase greenhouse gas emissions, which may be the key source of global warming. Furthermore, the cost of fossil fuel increases significantly with remoteness. By 2020, it is expected that Malaysia will discharge 285.73 million tons of CO_2. This means that CO_2 emission will increase by 68.86% compared to the amount of CO_2 emitted in 2000. Electric power generation alone contributes 43.40% of the total CO_2 released by Malaysia, which is the largest among all sectors [1,2]. In the previous Kyoto protocol, the Malaysian government signed for a reduction in CO_2. For this reason, the government is very concerned about the related environmental issue and wants to reduce the overall CO_2 emission. Therefore, island electrification using renewable energy sources in Malaysia is an important way to meet the challenge.

Among the various renewable energy sources, wave energy is the most promising environmental friendly clean and renewable energy source. It has a greater potential than any other power source to solve global energy problems. Extensive research on the idea of wave energy has been conducted since the oil crisis in the year 1970s. But, the first patent of wave energy extraction was recorded in the late eighteenth century [3]. Many WECSs have been patented and new patents are granted each month [4], which are based on nine basic techniques. These nine basic techniques are cavity resonators or oscillating water column (OWC), heaving and pitching bodies, pressure devices, particle motion converters, surging wave energy converters, Russell's rectifier, Cockerell's rafts, Salter's duck, and wave focusing techniques [3–6]. Among the various wave energy converters, OWC is generally considered as one of the most promising ocean wave energy conversion devices [7].

Unlike other green energy resources, wave energy can produce power all over the year. But, the high dependency on weather condition is the main drawback of the commercialize power generation from the wave energy source. An extensive review on the development of ocean wave energy conversion technologies shows that only 7% of the developing systems all over the world are pre-commercialized and there is no fully commercialized wave device developed yet [8]. A most recent design called "the Pelamis" (Sea Snake in Greek) was installed in the Aguçadora Wave Park near to Póvoa do Varzim; Portugal's northern coast is very much close to the full commercialization [8]. In reference [8–14], the authors only discussed about the design and development of wave energy devices, but they have not discussed about the intermittent power generation nature of wave energy source. Similarly, in references [15–17], the authors are also silent about this problem and they have not been paid much attention for a stand-alone system.

In this paper, a detail dynamic modeling, control, and simulation of a stand-alone wave energy supply system with maximum power point tracking (MPPT) is developed for islands communities. In the autonomous system, OWC wave energy device is used to generate the electric power from the sea waves. A MPPT algorithm is developed by controlling a boost converter at generator-side end. Using a DC–DC bidirectional buck-boost converter (DBBC), a control algorithm is developed between the dc-link and battery bank to maintain the constant dc-link voltage, and a switch-mode voltage source inverter (VSI) with complex vector control scheme is placed at the load-side end to control the load-side voltage. In addition, a simple passive L–C filter is placed after the inverter at the load-side end to eliminate the unwanted high-frequency harmonics, which are generated by the VSI based on the inverter switching frequency.

This simulation model can be used not only for investigating the stand-alone wave energy supply system performance with MPPT, but also for sizing and designing the stand-alone wave energy system to meet the system load demands under any available wave condition. In addition, results obtained from simulation are described to verify the effectiveness of the proposed system under the transient as well as steady-state load and wave conditions.

The sequential workflow hints of this paper are as follows: the complete mathematical modeling of OWC wave energy device has been presented with the necessary equations shown in Section 2. In addition, Sections 2 describes MPPT algorithm, the dc-link voltage control algorithm, and complex vector control scheme for load-side VSI. In Section 3, the Perhentian Islands is considered as a potential area for generating electric power from wave source based on the collected meteorological data. Section 4 presents all the necessary simulation results and discussions to check the performance of the proposed system. Finally, in Section 5, a conclusion is drawn by combining all the key points of the study.

2. System description

In this section, the detailed dynamic modeling of each component of the proposed overall stand-alone wave energy supply system is briefly described. The proposed stand-alone system consists of an OWC wave energy conversion device, a battery bank, a DBBC dc-link voltage controller with proportional integral (PI) control duty cycle, and a pulse-width modulation (PWM) VSI located at the load-side end. The OWC wave energy system consists of a Darrieus turbine with a permanent magnet synchronous generator (PMSG), an AC–DC three-phase uncontrolled rectifier, and a generator-side DC boost converter with a MPPT algorithm. Fig. 1 shows the complete block diagram of the stand-alone wave energy supply system.

2.1. Modeling and characteristics of OWC

OWC works much like a wind energy system. It uses movement of the water as a piston in a sealed chamber, which causes the rise and fall of the water level within the wave chamber. This cause creates pressure oscillations within the chamber, which can be used to drive a bidirectional wave turbine. The bidirectional turbine extracts the kinetic energy of sea wave and turned it into mechanical energy which is fed into the electrical generator. The generator converts this mechanical energy into electrical energy which will either feed directly to the load or in the grid.

It should be noted that this paper only focuses on the development of a battery storage stand-alone wave energy supply system and its MPPT algorithm for island communities. Therefore, power developed by the OWC with MPPT modeling is described here. The detailed design and complete mathematical modeling of OWC wave energy system can be found in reference [2,8,10–12,14,18,19], where more precise model is established.

As mentioned earlier, OWC wave energy operating principle is much like wind turbine system. The power available at the wave turbine consists of two terms: air velocity term P_a and air pressure term P_{pt}. Therefore, the total chamber power can be described using the following equation

$$\text{Chamber power } P_{in} = P_a + P_{pt} \tag{1}$$

where the power P_a and P_{pt} acting on the turbine due to the air velocity and pressure term as:

$$P_a = \frac{\rho A_2 V_2^3}{2} \tag{2}$$

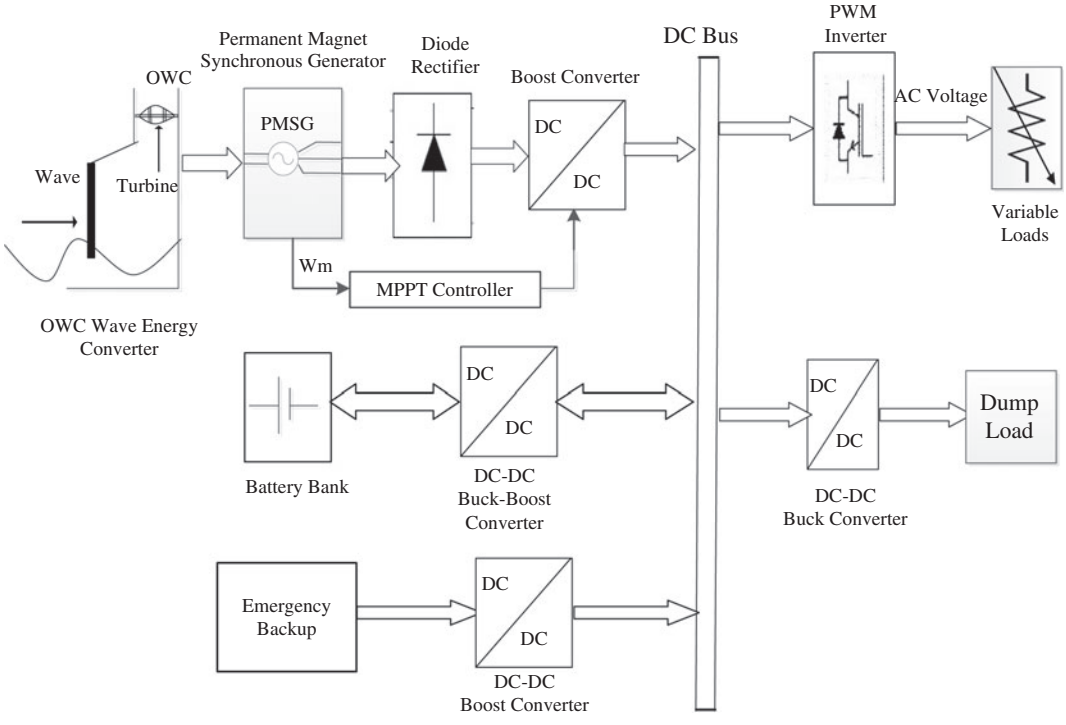

Fig. 1. Block diagram of the proposed stand-alone wave energy supply system.

and

$$P_{\mathrm{pt}} = \left[-\frac{A_1}{A_2}\frac{H_{\mathrm{in}}^2}{\theta^2}\omega^2\{2\cos(\omega t)^2 - 1\} \times \sin^2(\theta/2) + \frac{Q}{A_2}(V_2 - V_1)\right] \times Q \times \rho \tag{3}$$

The output available power developed by the OWC (power delivered by the turbine rotor) is a function of the turbine power coefficient C_{P}, so the total output power developed by the OWC is as follows:

$$P_{\mathrm{total}} = \left(\left\{\left[-\frac{A_1}{A_2}\frac{H_{\mathrm{in}}^2}{\theta^2}\omega^2\{2\cos(\omega t)^2 - 1\} \times \sin^2(\theta/2) + \frac{Q}{A_2}(V_2 - V_1)\right] \times Q \times \rho\right\} + \frac{\rho A_2 V_2^3}{2}\right) \times C_{\mathrm{P}} = \left(\left\{\left[-\frac{A_1}{A_2}\frac{H_{\mathrm{in}}^2}{\theta^2}\omega^2\{2\cos(\omega t)^2 - 1\} \times \sin^2(\theta/2) + \frac{Q}{A_2}\left(\frac{\omega_{\mathrm{m}} R}{\lambda} - V_1\right)\right] \times Q \times \rho\right\} + \frac{\rho A_2 \omega_{\mathrm{m}}^3 R^3}{2\lambda^3}\right) \times C_{\mathrm{P}}(\lambda, \beta) \tag{4}$$

where H_{in} is the averaged internal wave height (WH) (m), A_1 is the flow surface area of the chamber (m^2), A_2 is the inlet turbine area (m^2), ρ is the air density (kg/m^3), Q is the air flow rate across the turbine, ω is the angular velocity of the sea wave, V_1 is the air flow velocity inside the chamber (m/s), V_2 is the turbine inlet velocity (m/s), θ is the angular chamber length (m), ω_{m} is the angular velocity of wave turbine rotor (rad/s), λ is the tip-speed ratio, β is the pitch angle, and R is the radius of Darrieus turbine. C_{P} is only function of λ when β is equal to zero indicated in Eq. (5) [20], and also power conversion rate performance of a Darrieus wave turbine is influenced by λ shown in Eq. (6).

$$C_{\mathrm{P}}\ (\lambda) = \frac{55.04 - 4.69\lambda}{\lambda} e^{\left(\frac{-21 + 0.735\lambda}{\lambda}\right)} + \frac{0.0068\lambda}{1 - 0.035\lambda} \tag{5}$$

and

$$\lambda = \frac{\omega_{\mathrm{m}} R}{V_2} \tag{6}$$

Based on the Eq. (5), the relation between C_{P} and λ shown in Fig. 2. It can be noticed from that for λ equal to 7.4, the optimum value of C_{P} is about 0.4. It means Darrieus turbine extracts maximum power when it operates at maximum C_{P} (i.e. at $C_{\mathrm{P\text{-}opt}}$). Therefore, it is important to keep the rotor speed of Darrieus turbine at an optimum rage of the λ with varying WH and wave period (WP).

Using Eqs. (4) and (6), the target optimum power and torque of the Darrieus wave turbine can be expressed as:

$$P_{\mathrm{total-opt}} = \left(\left\{\left[-\frac{A_1}{A_2}\frac{H_{\mathrm{in}}^2}{\theta^2}\omega^2\{2\cos(\omega t)^2 - 1\} \times \sin^2(\theta/2) + \frac{Q}{A_2}\left(\frac{\omega_{\mathrm{m-opt}} R}{\lambda_{\mathrm{opt}}} - V_1\right)\right] \times Q \times \rho\right\} + \frac{\rho A_2 \omega_{m-\mathrm{opt}}^3 R^3}{2\lambda_{\mathrm{opt}}^3}\right) \times C_{\mathrm{P-opt}} \tag{7}$$

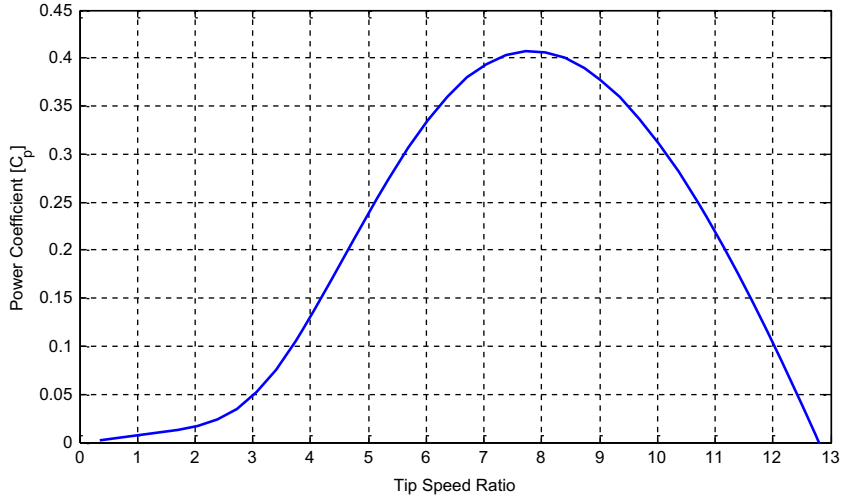

Fig. 2. The relation between C_{P} and λ of Darrieus turbine.

and

$$T_{\text{opt}} = \frac{\left(\left\{\left[-\frac{A_1}{A_2}\frac{H_{\text{in}}^2}{\theta^2}\omega^2\{2\cos(\omega t)^2 - 1\} \times \sin^2(\theta/2) + \frac{Q}{A_2}\left(\frac{\omega_{\text{m-opt}}R}{\lambda_{\text{opt}}} - V_1\right)\right] \times Q \times \rho\right\} + \frac{\rho A_2 \omega_{\text{m-opt}}^3 R^3}{2\lambda_{\text{opt}}^3}\right) \times C_{\text{P-opt}}}{\omega_{\text{m-opt}}} \tag{8}$$

where

$$\omega_{\text{m-opt}} = \frac{\lambda_{\text{opt}} V_2}{R} \tag{9}$$

The mechanical power developed by the Darrieus wave turbine is a function of the rotor mechanical speeds for different WHs and periods as shown in Fig. 3 and this figure also indicates the optimum power. The maximum power can be extracted from the wave turbine if the controller can properly follow the optimum curve shown in Fig. 3.

2.2. Control of generator-side converter with MPPT

Fig. 4 shows the control structure of the generator-side converter. The main control objective of this controller is to control the duty cycle of the generator-side DC–DC boost converter which is shown in Fig. 5 to extract maximum power from variable wave condition. The control algorithm follow the below steps:

(1) Calculate generator speed ω_g.
(2) Determine the reference torque using the below equation:

$$T_{\text{g-ref}} = \frac{\left(\left\{\left[-\frac{A_1}{A_2}\frac{H_{\text{in}}^2}{\theta^2}\omega^2\{2\cos(\omega t)^2 - 1\} \times \sin^2(\theta/2) + \frac{Q}{A_2}\left(\frac{\omega_g R}{\lambda_{\text{opt}}} - V_1\right)\right] \times Q \times \rho\right\} + \frac{\rho A_2 \omega_g^3 R^3}{2\lambda_{\text{opt}}^3}\right) \times C_{\text{P-opt}}}{\omega_g} \tag{10}$$

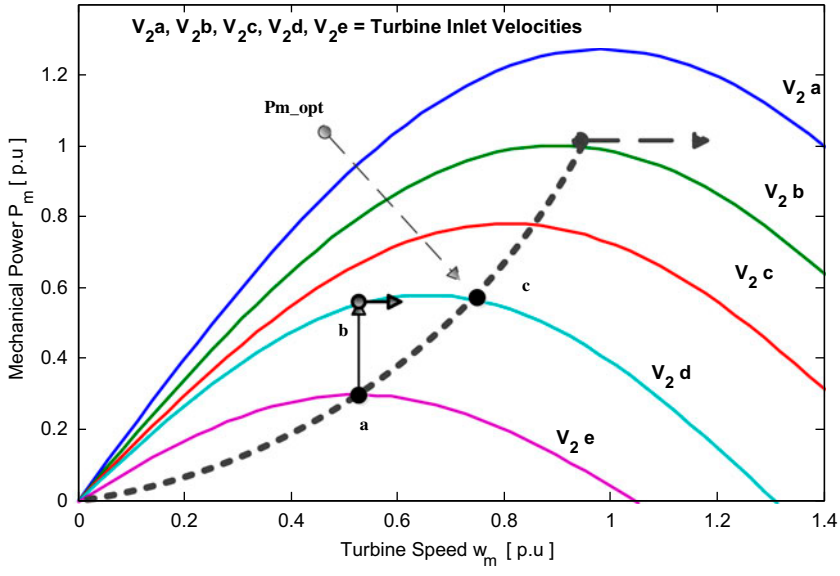

Fig. 3. The relation between the mechanical power and rotor mechanical speeds of a Darrieus wave turbine for different WH and periods.

(3) This reference torque is used to calculate the reference DC current using the rectifier voltage V_{dr} as given by:

$$I_{dr-ref} = \frac{T_{g-ref} \times \omega_g}{V_{dr}} \quad (11)$$

(3) The error between the measured DC current and DC reference current is used to control the duty cycle of the generator-side converter through a PI controller to extract the maximum power from the wave turbine.

The acceleration or deceleration of the PMSG is determined by the difference between the generator torque T_m and turbine torque T_g. If the PMSG speed is higher than the optimal speed, then turbine torque is less than the PMSG torque and the PMSG will be decelerated. The PMSG will be accelerated if the PMSG speed is less than the optimal speed. For describing this MPPT control function, consider Fig. 3. If the PMSG operating at point "a" and turbine inlet speed increases from V_{2e} to V_{2d} (point "b"), the additional 00power and hence torque causes the PMSG to accelerate and also causes the difference between the

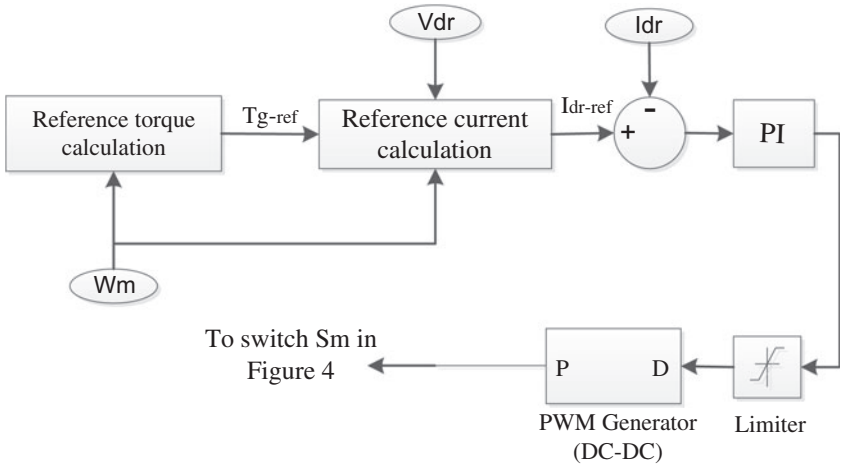

Fig. 4. The control algorithm of the generator-side converter for MPPT [26].

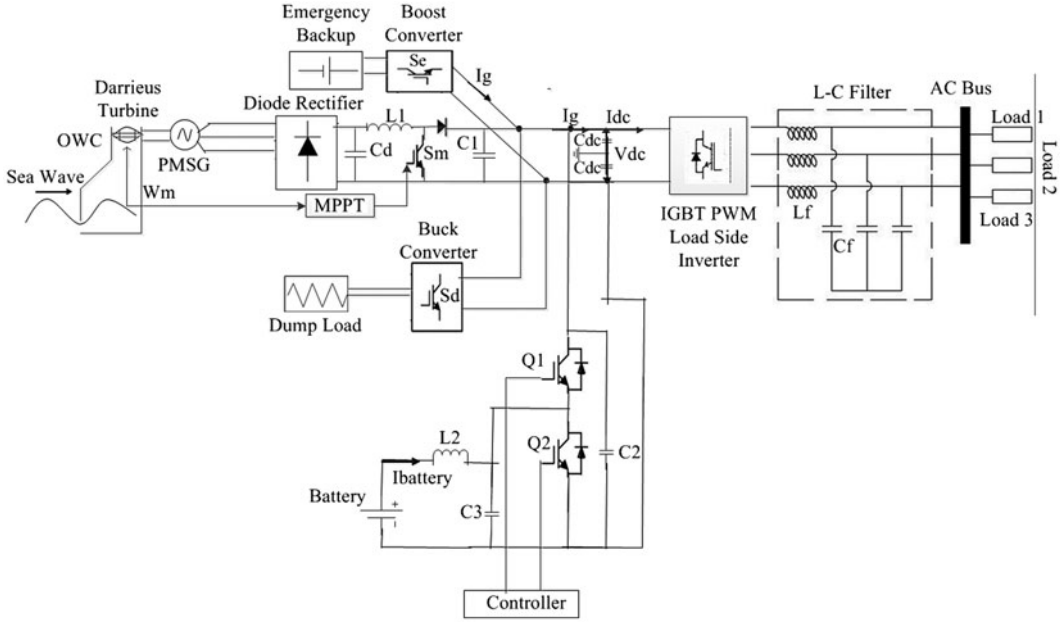

Fig. 5. The complete model of the proposed stand-alone wave energy supply system.

measured DC current and DC reference current; this difference is used to control the duty cycle of generator-side converter to extract the maximum power. The accelerating torque is the difference between the turbine mechanical torque and the torque given by the optimum curve. Finally, the PMSG will reach the point "c" where the difference between of the torque is zero. A similar situation occurs when the turbine inlet velocity decreases based on WH and WP. In the proposed MPPT method, the turbine inlet velocity is no need to monitored using mechanical sensor.

2.3. Dc-link voltage control

In this proposed system, a neutral wire is inserted between the dc-link capacitors which are connected before the VSI for feeding the single-phase load as well as the three-phase loads, shown in Fig. 5.

In this paper, the dc-link side is connected to a battery bank through DBBC; the main objective of the DBBC control is to maintain a constant dc-link voltage as a reference value and discharge/charge current from/to the battery bank according to the required load power. The battery bank DBBC controller schematic diagram is shown in Fig. 6. The battery bank voltage can be kept lower as compared to the dc-link reference voltage (V_{dc}^{*}) using DBBC and so a smaller number of battery are required to be connected in series. In the proposed system, the battery bank voltage is kept at around 300 V whereas $V_{dc}^{*} = 650$ V. In this study, the depth of discharge of the battery bank is considered to be 60% [2,21–23]. In addition, it is assumed that it should provide electric power to the 2.5 kW load for approximately an hour when the generated wave power is zero. The detailed calculation of the battery bank rating is discussed in Appendix I.

In Fig. 4, the value of the switching frequency, inductor, and capacitors used in DBBC is important for its conduction mode operation of it [2,24,25]. The inductor used in the battery bank side shows the lower ripple current results, which increases the lifetime and efficiency of the battery bank. Conduction mode operation of DBBC also depends on input and output current. The value of the inductor and capacitors are as follows [2]:

$$\text{Inductance } L_2 = \frac{V_{\text{Battery}} \times (V_{\text{dclink}} - V_{\text{Battery}})}{I_{\text{Battery}} \times f_s \times V_{\text{dclink}}} \tag{12}$$

$$\text{Buck mode capacitance } C_2 = \frac{k_L \times I_{\text{Battery}}}{8 \times f_s \times V_{\text{Battery(ripple)}}} \tag{13}$$

and

$$\text{Boost mode capacitance } C_3 = \frac{D_{\text{Boost}} \times I_{\text{dclink}}}{f_s \times V_{\text{dclink(ripple)}}} \tag{14}$$

where V_{Battery} is the voltage of the battery bank, I_{dclink} is the dc-link current, V_{dclink} is the dc-link voltage, $V_{\text{dclink(ripple)}}$ is the boost side output desired ripple voltage, $V_{\text{Battery(ripple)}}$ is the buck side output desired ripple voltage, f_s is the switching frequency, k_L is the estimated coefficient of indicator ripple current at buck side, and I_{Battery} is the battery bank current.

The battery bank, in this paper, can act either as a sink or as a power supply. As a result, due to the weather conditions, it should charge or discharge within specified limits when there is surplus or a lack of wave power. In this study, the surplus power due to the high wave power condition initially supply to the battery bank until its upper limit charge carrying capacity and after that the dump load absorbs the additional power. The dump load controlled via the chopper control is shown in Fig. 7. In this case, the controller switching decision is made by comparing the present status and upper limit of state of charge (SOC).

The battery bank may not able to meet the system load demand at each instance in case of long-term or

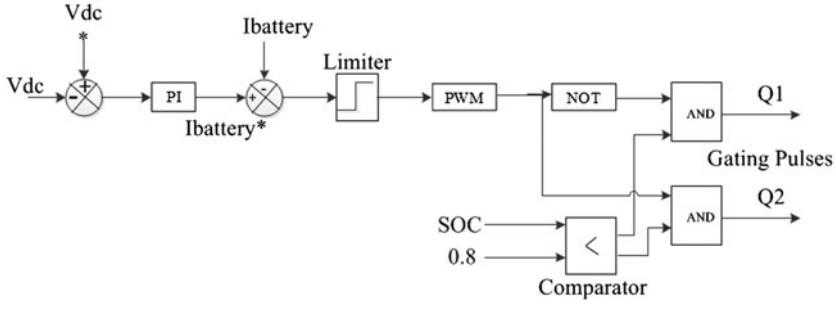

Fig. 6. The schematic diagram of DBBC converter controller.

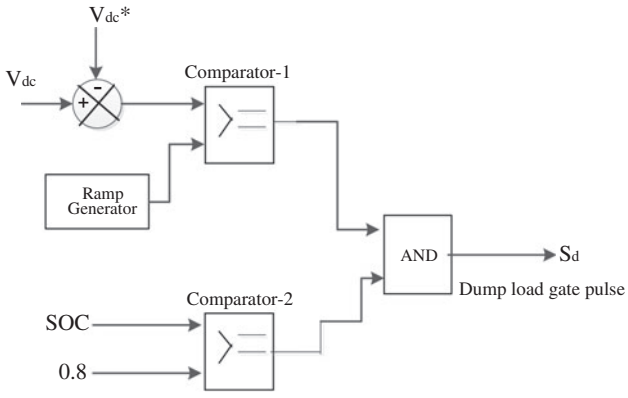

Fig. 7. The schematic diagram of dump load controller.

lower wave power conditions. For this reason, an emergency backup is integrated with the proposed stand-alone system in this paper. The control algorithm of the emergency backup is shown in Fig. 8. A flow chart is depicted in Fig. 9 based on the above control coordination among the wave sources, battery, emergency backup, and dump load, where the lower and upper limit of SOC of the battery bank is kept at 0.2 and 0.8, respectively.

2.4. Load-side VSI control

A three-phase space vector control VSI is used at the load end as an interface element between the dc-link voltage and the system load. It is used to

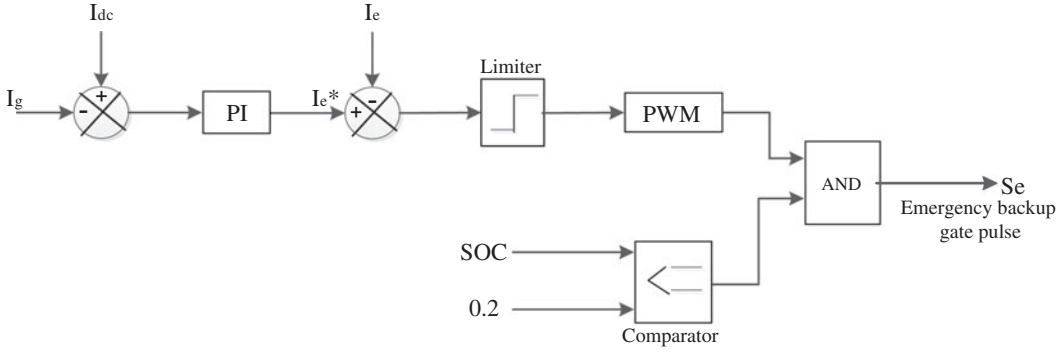

Fig. 8. The schematic diagram of emergency backup controller.

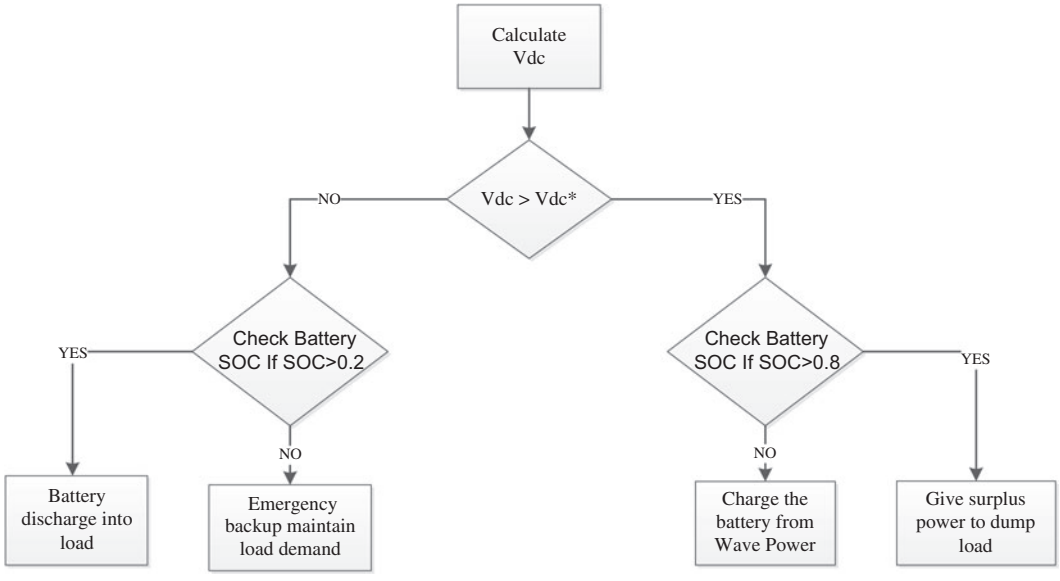

Fig. 9. Dc-link voltage control algorithm.

control the voltage and frequency at the system load end. In this study, the system load voltages should be controlled in terms of voltage amplitude and frequency because there is no power grid connection. The space vector control method is used to control the system output voltage during the variation in required wave power or load power.

Based on the synchronously rotating frame described in [26], the space vector control technique is used in this proposed system. The three-phase I_a, I_b, I_c currents and V_a, V_b, V_c voltages should be measured and transformed from the stationary reference *a-b-c* frame to the rotating reference *d-q* frame using the preferred output load voltage frequency. In this paper, the specified output phase voltage root mean square (RMS) value and the frequency are 220 V and 50 Hz, respectively.

The equations of voltage using reference rotating *d–q* frame transformation are taken from [26]:

$$v_d = v_{di} - L_f \frac{di_d}{dt} + L_f \omega i_q \tag{15}$$

$$v_q = v_{qi} - L_f \frac{di_q}{dt} - L_f \omega i_d \tag{16}$$

Using the *d–q* reference rotating frame transformation, the active and reactive power is given by:

$$\text{Active power } P = \frac{3}{2}(v_d i_d + v_q i_q) \tag{17}$$

$$\text{Reactive power } Q = \frac{3}{2}(v_d i_q + v_q i_d) \tag{18}$$

The active and reactive power equations will be as follows if the reference rotating frame is as $v_q = 0$ and $v_d = \mid V \mid$:

$$P = \frac{3}{2} v_d i_d = \frac{3}{2} |V| i_d \tag{19}$$

$$Q = \frac{3}{2} v_d i_q = \frac{3}{2} |V| i_q \tag{20}$$

Therefore, the active and reactive power can be controlled by controlling direct and quadrature current elements, respectively. And for the resistive load case, V_d^* can be expressed as:

$$V_d^* = \sqrt{2} V_{RMS}^* \tag{21}$$

where V_{RMS}^* is the RMS reference value of the output phase voltage. In this control technique, internal control loops output current and external control loops output voltages are regulated by PI controllers. In this

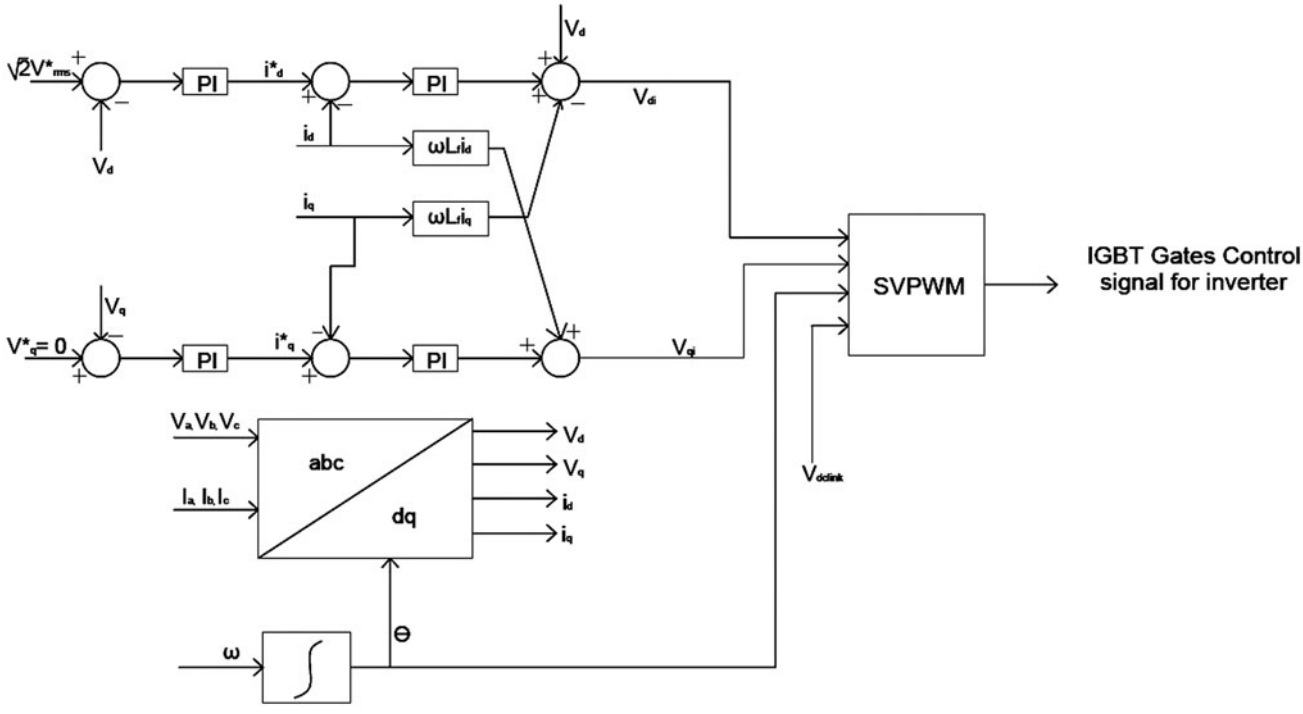

Fig. 10. The three-phase load-side VSI controller.

paper, the Ziegler–Nichols tuning method is used for regulating all the PI controllers [27]. The control technique of the load-side VSI is depicted in Fig. 10.

Based on the switching frequency of the inverter, the unwanted high-frequency harmonics will generate in output AC voltage by the VSI, which ultimately creates power quality problem in the consumer end. Space vector PWM technique is used in this controller, because it slightly reduces the harmonics contents in the output voltage. And also, it increases the fundamental output voltage. To reduce the unwanted high frequency harmonics for avoiding the power quality problem in the customer end, a simple passive L–C filter is used in the load-side end. The passive L–C filter design [2] is given in Appendix II and the values are:

$$L_f = 0.052 \text{ H}$$

$$C_f = 2\ \mu\text{F}$$

2.5. Modeling of battery

In this paper, a typical battery model [28] is implemented. This model uses only the SOC of the battery as a state variable to avoid the algebraic loop problem. In addition, the model developed [28] can precisely characterize four types of battery chemistry including lead–acid battery.

In this paper, the battery is modeled using a controlled series connected voltage source with a constant resistive value, shown in Fig. 7, where the controlled voltage source is expressed by the following equation [28]:

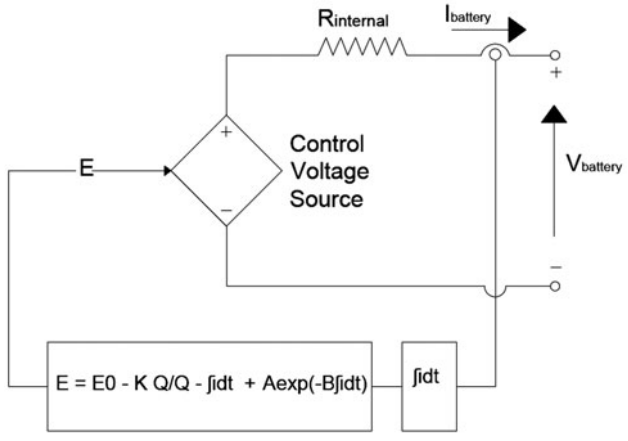

Fig. 11. Nonlinear typical battery model [28].

$$E = E_0 - K\frac{Q}{Q - \int i\mathrm{d}t} + A\exp\left(-B\int i\mathrm{d}t\right) \quad (22)$$

$$V_{\text{Battery}} = E - R_{\text{in}}I_{\text{Battery}} \quad (23)$$

where E_0 is the no load voltage of the battery (V), Q is the battery capacity (Ah), K is the polarization voltage (V), A is the exponential zone amplitude (V), V_{Battery} is the battery voltage (V), B is the exponential zone time constant inverse $(\text{Ah})^{-1}$, R_{in} is the internal battery resistance (Ω), $\int i\mathrm{d}t$ is the charge drawn and supplied by the battery (Ah), and I_{Battery} is the battery current (A) (Fig. 11).

Based on Eq. (22), the typical battery model is developed in MATLAB/Simulink and connected to a DBBC using controlled voltage source.

3. Site selection

Malaysia is surrounded by sea and its latitude and longitude is 2˚-30´˚N and 112˚-30´˚E. It has a total of 878 islands [29–32]. In Malaysia, Perhentian Island (shown in Fig. 12) is one of the most popular islands resort. Geographically, Perhentian Island or Pulau Perhentian is a hot and humid island with rain all year round. It is approximately 20 km off the northeastern coast of West Malaysia in the state of Terengganu. It is a resort island and there is only one village inhabited by the locals. Diesel generators are the main source of electric power. On this island, the National Energy Policies and University Kebangsaan Malaysia installed a solar-wind hybrid energy system in 2007 [33]. It was not connected to the electrical network because of its weak hybrid power management strategy during periods of lower wind and solar irradiation conditions. The winds are rare in this area and also PV efficiency decreases due to the humidity affect.

As an island surrounded by the sea, wave energy can be considered as one of the efficient power generation sources in Perhentain Island. The wave data of Perhentain Island are shown in Fig. 13, where the average peak WH and WP occur from November to January. The wave data of the Perhentain Island are collected from Malaysian Meteorological Department Labuan (MMDL). In addition, the collected wave data are analyzed by the "hindcast" technique [35]. MMDL measured wave data using voluntary observation ship Scheme and acoustic doppler current profiler equipment.

At this site, the maximum and minimum average WH measured in November (WH = 2.1 m) and June (WH = 0.88 m). On the other hand, the maximum and minimum average WP measured in December

Fig. 12. Location of target site (Perhentian Island) (modified from [34]).

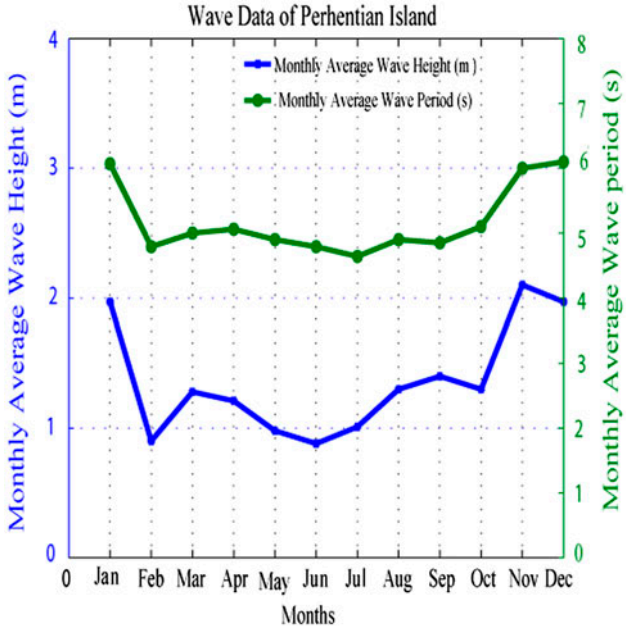

Fig. 13. Monthly average WH/WP data of a year for Perhentian Island.

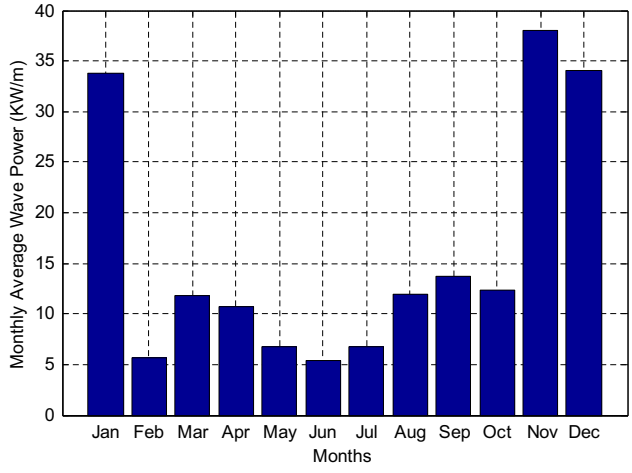

Fig. 14. Average wave power level of a year for Perhentain Island.

(WP = 6.1 s) and July (WP = 4.64 s). The power generated by the wave during the whole year is shown in Fig. 14, and it is mainly depend on the WH and WP according to the wave theory and equations in reference [1,2].

Malaysian sea has an average 8.5 kW/m wave power level [1]. With reference to above Fig. 14, it could be said that Perhentain Island site is economically viable for commercial scale wave power generation in Malaysia, because it has an average 15.9 kW/m wave power level. Because any wave power site are

able to produce electric power at competitive prices if it has an average wave power level equal or above 15 kW/m. In addition, these sites are considered to have an exceptionally high-energy resources than other renewable energy source like wind and solar.

4. Simulation result and discussion

The simulation model of the proposed stand-alone wave energy supply system with energy storage has been modeled using Matlab/Simulink environment under the different wave and load conditions. In this study, PMSG is modeled in Matlab/Simulink from the literature [36–38] and the parameters of it are taken from [39], which are presented in Appendix III. The parameters of the OWC and Darrieus turbine are also mentioned in Appendix III. In this section, the average WH and WP for February, March, and June from Section 3 is used to test the performance of the proposed stand-alone system under the following conditions. In this simulation study, 20 μs time is used for sampling during the simulation.

Figs. 15 and 16, respectively, show that the value of power coefficient and the wave power at different steps. It is clear from both figures that simple MPPT control technique without any mechanical sensor

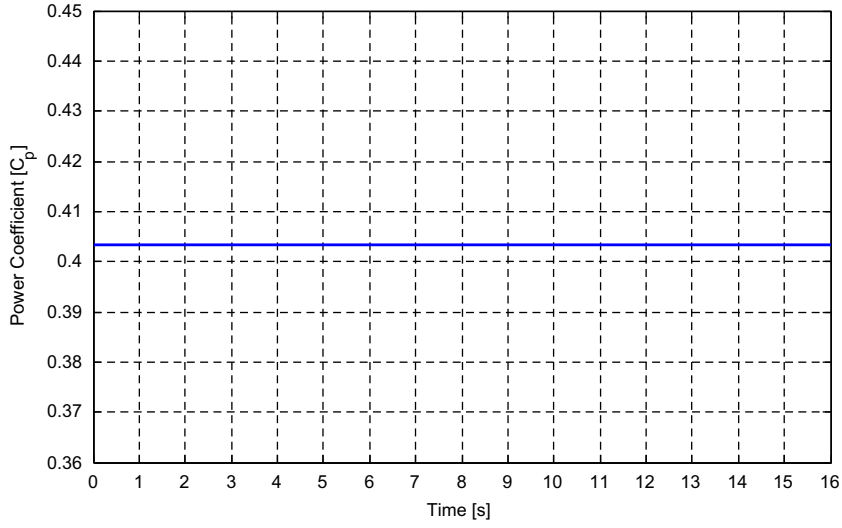

Fig. 15. Power coefficient of Darrieus turbine during the whole simulation.

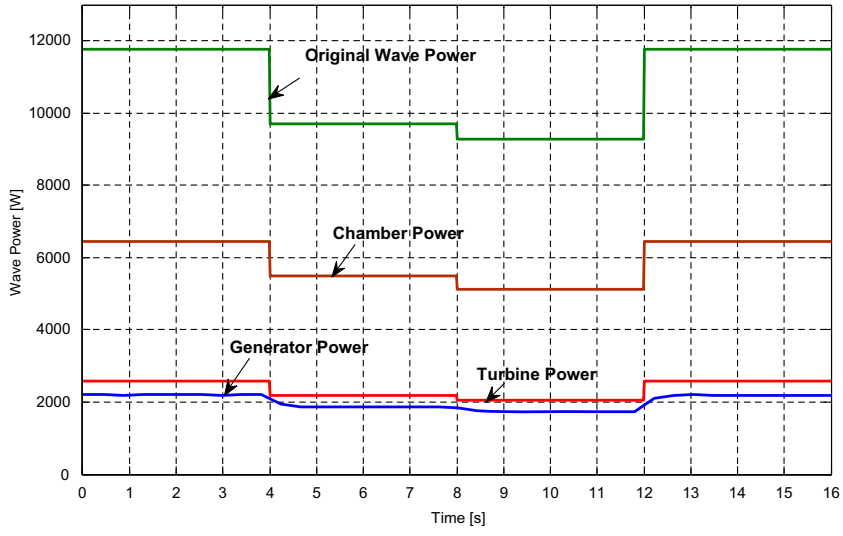

Fig. 16. Developed wave power at different steps.

works well, where the C_P value is kept at its optimum value which approximately equals 0.40 with varying wave and load condition to extract maximum power from available WH and WP. The simulation results of the MPPT control algorithm demonstrate that the controller can be able to extract maximum power from the variable speed wave turbine under the fluctuating WH and WP.

The performance of dc-link voltage controller is presented in Fig. 17. Fig. 17 shows the active power distribution curve of generated wave power, load demand, and battery bank power. From Fig. 17, it can be seen that the performance of the dc-link DBBC voltage controller is quite satisfactory because the power from the battery bank changes (charges/discharges) in order to maintain system power stability under varying wave and load conditions. So, it is clear that the dc-link DBBC voltage controller is able to discharge the battery bank into the load when the load power is more than the generated wave power and also the controller is able to charge the battery bank when the load power is less than the generated wave power.

Furthermore, it can also maintain the constant dc-link voltage at 650 V during the change in wave and load power, as shown in Fig. 18. But it shows insignificant deviation when there is a variation in

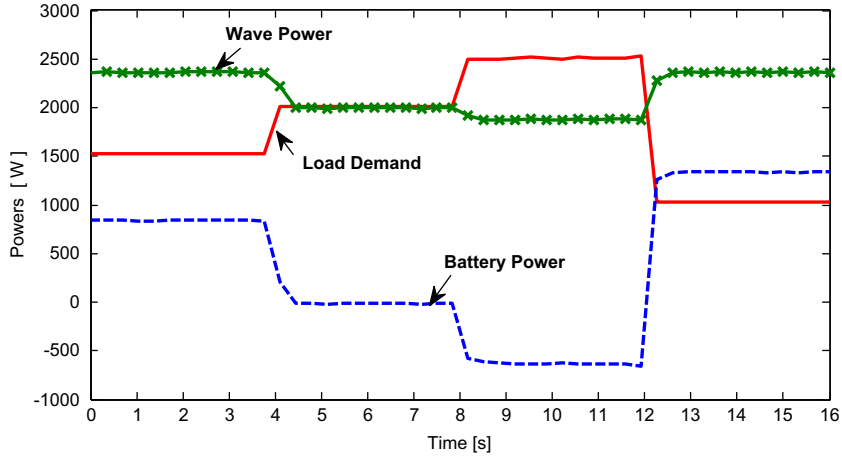

Fig. 17. Active power distribution curve of the stand-alone wave energy supply during the variation in wave power with variable load.

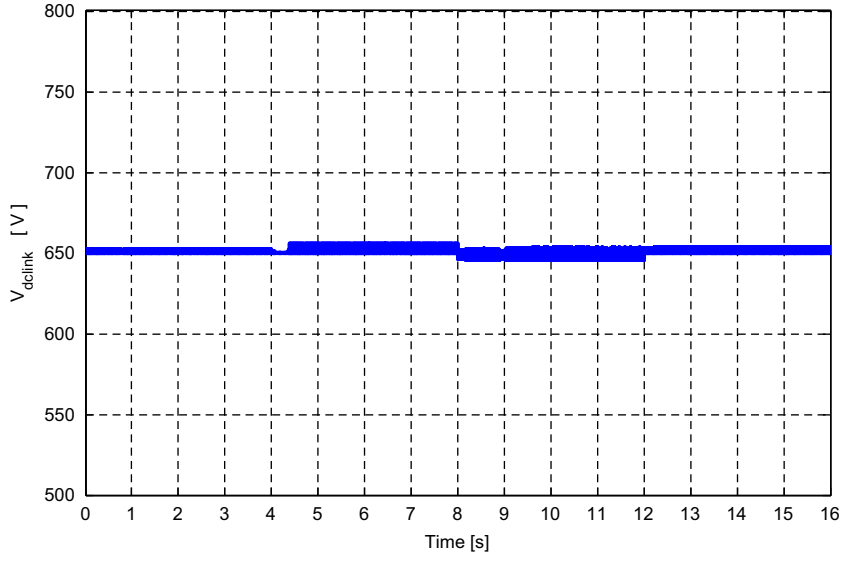

Fig. 18. Dc-link voltage of the stand-alone wave energy supply system during the variation in wave power with variable load.

load. This is because of the appreciable delay between wave and load power changes. In this case, wave and battery bank power satisfactorily meets the system load demand at each instant. Therefore, it can be established that controller performance is quite acceptable in a steady state as well as in transient wave and load power conditions.

The output line current response of the above conditions during the long-time simulation is shown in Fig. 19. The output line current varying in Fig. 19 because load is varying in this case. Fig. 19(b) and (c) show the output line current when the load power increase at simulation time from 7.95 to 8.05 s and when the load power decrease at simulation time 11.96 to 12.06 s, respectively. For above condition, output line voltage for whole simulation time is shown in Fig. 20. With reference to Fig. 20, it is seen that the VSI controller shows satisfactory performance, because it maintains voltage stability in load side during the

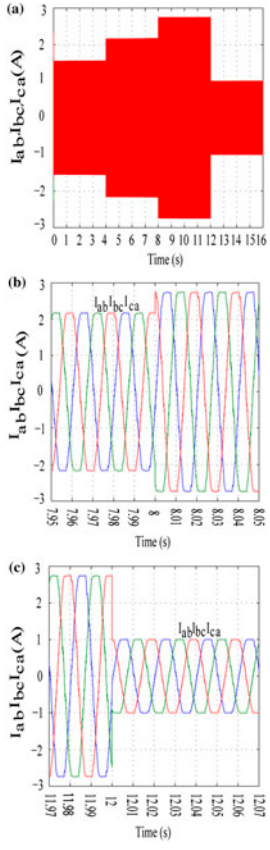

Fig. 19. Output line current response with change in required load power. (a) Output line currents throughout the full simulation time; (b) Output line current when the load increases at simulation time from 7.95 to 8.05 s; (c) Output line current when the load decreases at simulation time from 11.96 to 12.06 s.

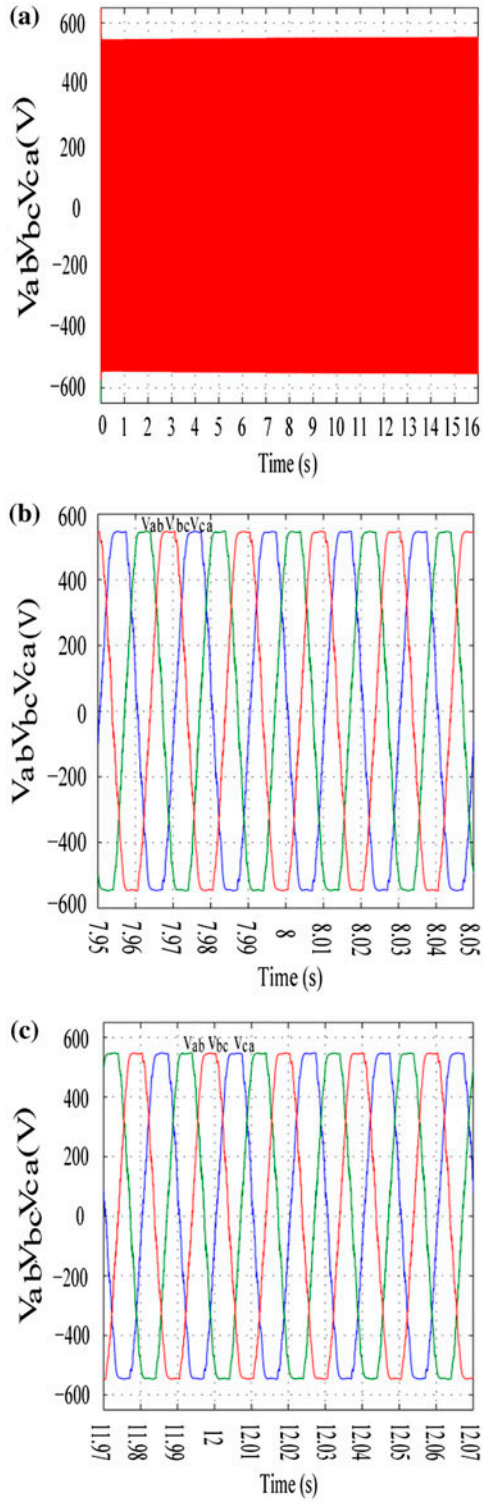

Fig. 20. Output line voltage response with change in required load power. (a) Output line voltage throughout the full simulation time; (b) Output line voltage when the load increases at simulation time 7.95 to 8.05 s; (c) Output line voltage when the load decreases at simulation time 11.96 to 12.06 s.

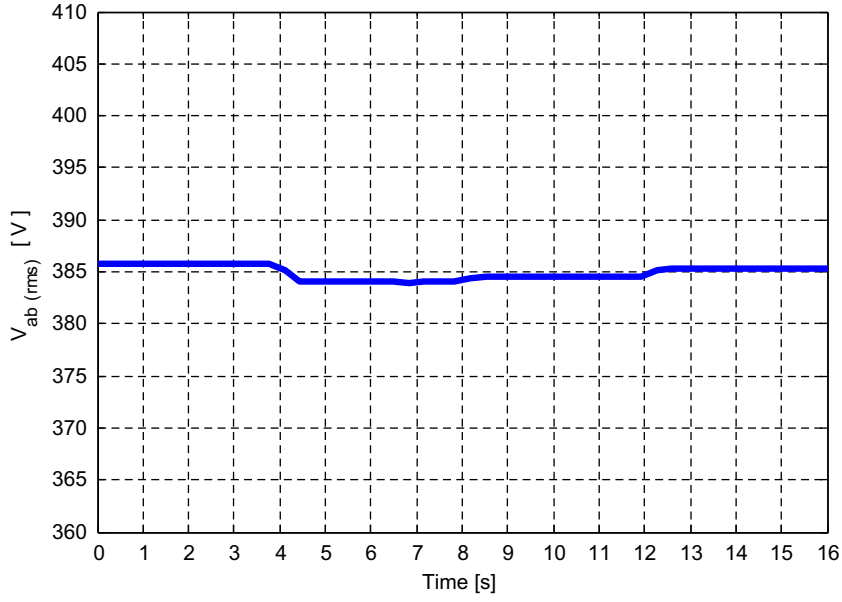

Fig. 21. The output RMS phase voltage during the variation in wave power with variable load.

wave and load power variation. Fig. 21 shows the output RMS line voltage (for line V_{ab}) where it is maintained at 385 V as a reference value. The total harmonics distortion in the output voltage and current at load side is about 1.7 and 1.55%, respectively, which illustrates the good quality of the voltage and current generated at the load-side end.

Based on the above simulation results, it can be concluded that the proposed stand-alone system is be able to deliver a suitable quality of voltage and current to the load with the help of inverter switching and a passive L–C filter. It could be found from the literature in reference [1,3,4,6,8,10–12] that the overall efficiency of the OWC varies from 10–15% according to the chamber and turbine design. But in this analysis, it can found that the OWC efficiency is almost 18.5% for the proposed hybrid system. Finally, it has been established that the proposed stand-alone system can successfully accommodate WH, WP, and load changes, and the MPPT algorithm can efficiently extract the maximum wave power during the load changes.

5. Conclusion

A stand-alone wave power generation system with MPPT and an appropriate power management algorithm has been designed and modeled in this paper for remote island uses in the absence of electric power grid. The power available from wave energy source is highly dependent on weather conditions such as WH and WP. In this paper, an OWC wave energy system integrated with a battery bank using a novel topology to overcome this deficiency. And also a generator-side boost converter controller is able to extract the maximum power by keeping C_P value at its optimum value with varying wave and load condition. This stand-alone topology shows excellent performance under varying load power requirement, WH and WP where wave data are based on real-world records. Based on the simulation results and analysis, it could be concluded that the proposed stand-alone system can be satisfactorily used in the Pehentian Islands. Future work should aim at setting up the proposed stand-alone wave energy supply system in the University of Malaya laboratory to verify the simulation results.

Conflict of interests

The authors declare that there is no conflict of interests regarding the publication of this article.

Acknowledgments

The authors would like thanks to the KeTTHA, Ministry of Energy, Green Technology and Water (53-02-03-1102) and the Postgraduate Research Fund, University of Malaya (PG085-2013B) for providing financial support.

References

[1] N.H. Samrat, N.B. Ahmad, I. Choudhury, Z. Taha, Prospect of wave energy in Malaysia, in: Power Engineering and Optimization Conference (PEOCO), 2014 IEEE 8th International, IEEE, Langkawi, Malaysia, 2014, pp. 127–132.

[2] N.H. Samrat, N.B. Ahmad, I.A. Choudhury, Z.B. Taha, Modeling, control, and simulation of battery storage photovoltaic-wave energy hybrid renewable power generation systems for island electrification in Malaysia, Sci. World J. 2014 (2014) 1–21.

[3] A. Muetze, J. Vining, Ocean wave energy conversion-A survey, in: Industry Applications Conference, 2006. 41st IAS Annual Meeting. Conference Record of the 2006 IEEE, IEEE, Florida, FL, USA, 2006, pp. 1410–1417.

[4] M.E. McCormick, Ocean Wave Energy Conversion, Courier Dover Publications, Mineola, NY, 2013.

[5] Z. Chen, H. Yu, M. Hu, G. Meng, C. Wen, A review of offshore wave energy extraction system, Adv. Mech. Eng. 2013 (2013) 1–9.

[6] J. Halliday, D. Dorrell, Review of wave energy resource and wave generator developments in the UK and the rest of the world, in: IASTED EuroPES conference, ACTA Press, Rhodes, 2004.

[7] R.-S. Tseng, R.-H. Wu, C.-C. Huang, Model study of a shoreline wave-power system, Ocean Eng. 27 (2000) 801–821.

[8] M.-F. Hsieh, I.-H. Lin, D.G. Dorrell, M.-J. Hsieh, C.-C. Lin, Development of a wave energy converter using a two chamber oscillating water column, Sustain. Energy, IEEE Trans. 3 (2012) 482–497.

[9] L. Cameron, R. Doherty, A. Henry, K. Doherty, J. Van't Hoff, D. Kaye, D. Naylor, S. Bourdier, T. Whittaker, Design of the next generation of the Oyster wave energy converter, in: 3rd International Conference on Ocean Energy, Bilbao, Spain, 2010, pp. 1–12.

[10] D. Dorrell, W. Fillet, Investigation of a small-scale segmented oscillating water column utilizing a Savonius rotor turbine, in: Proceeding of International Conference on Energy and Environment (ICEE 2006), Selangor, Malaysia, 2006, pp. 23–32.

[11] D.G. Dorrell, M.-F. Hsieh, C.-C. Lin, A small segmented oscillating water column using a Savonius rotor turbine, IEEE Trans. Ind. Appl. 46 (2010) 2080–2088.

[12] D.G. Dorrell, M.-F. Hsieh, C.-C. Lin, A multichamber oscillating water column using cascaded Savonius turbines, IEEE Trans. Ind. Appl. 46 (2010) 2372–2380.

[13] M. Faizal, M.R. Ahmed, Y.-H. Lee, A design outline for floating point absorber wave energy converters, Adv. Mech. Eng. 2014 (2014) 1–18.

[14] K. Mala, J. Jayaraj, V. Jayashankar, T. Muruganandam, S. Santhakumar, M. Ravindran, M. Takao, T. Setoguchi, K. Toyota, S. Nagata, Design of a 50 GWh wave energy plant, in: India Conference (INDICON), 2009 Annual IEEE, IEEE, Gujarat, India, 2009, pp. 1–4.

[15] H. He, Q. Qu, J. Li, Numerical simulation of section systems in the pelamis wave energy converter, Adv. Mech. Eng. 2013 (2013) 1–8.

[16] L. Huang, M. Hu, J. Liu, C. Liu, W. Zhong, Design and analysis of a linear hybrid excitation flux-switching generator for direct drive wave energy converters, Adv. Mech. Eng. 2013 (2013) 1–11.

[17] Z. Shi, H. Yu, F. Marignetti, Performance analysis of a completely sealed double oscillating structure applied in wave energy extraction, Adv. Mech. Eng. 2013 (2013) 1–6.

[18] J. Falnes, Ocean Waves and Oscillating Systems, Cambridge University Press, Cambridge, 2002.

[19] I.G. Morrison, C.A. Greated, Oscillating water column modelling, Coastal Eng. Proc. 1 (1992) 502–511.

[20] M.M. Hussein, T. Senjyu, M. Orabi, M.A. Wahab, M.M. Hamada, Control of a stand-alone variable speed wind energy supply system, Appl. Sci. 3 (2013) 437–456.

[21] H. Bai, Y. Zhang, C. Semanson, C. Luo, C. Mi, Modelling, design and optimisation of a battery charger for plug-in hybrid electric vehicles, IET. Elec. Sys. Transp. 1 (2011) 3–10.

[22] C. Bhende, S. Mishra, S.G. Malla, Permanent magnet synchronous generator-based standalone wind energy supply system, Sustain. Energy, IEEE Trans. 2 (2011) 361–373.

[23] L. Wang, J. Liang, G. Xu, K. Xu, Z. Song, A novel battery charger for plug-in hybrid electric vehicles, in: Information and Automation (ICIA), 2012 International Conference, IEEE, Shenyang, China, 2012, pp. 168–173.

[24] H. Bai, C. Mi, Power electronics in battery management systems, in: Transients of Modern Power Electronics, John Wiley & Sons, Chichester, pp. 157–181.

[25] H. Bai, C. Mi, The impact of bidirectional DC-DC converter on the inverter operation and battery current in hybrid electric vehicles, in: Power Electronics and ECCE Asia (ICPE & ECCE), 2011 IEEE 8th International Conference, IEEE, Jeju, South Korea, 2011, pp. 1013–1015.

[26] M.E. Haque, M. Negnevitsky, K.M. Muttaqi, A novel control strategy for a variable speed wind turbine with a permanent magnet synchronous generator, in: Industry Applications Society Annual Meeting, 2008, IAS'08, IEEE, Edmonton, Canada, 2008, pp. 1–8.

[27] K.J. Åström, T. Hägglund, PID Controllers: Theory, Design, and Tuning, Instrument Society of America, Research Triangle Park, NC, 1995.

[28] O. Tremblay, L.-A. Dessaint, A.-I. Dekkiche, A generic battery model for the dynamic simulation of hybrid electric vehicles, in: Vehicle Power and Propulsion Conference, 2007, VPPC 2007, IEEE, IEEE, Arlington, TX, USA, 2007, pp. 284–289.

[29] Geography of Malaysia, Wikipedia, 2013, [Online]. Available from: http://en.wikipedia.org/wiki/Geography_of_Malaysia.

[30] List of islands of Malaysia, Wikipedia, 2013, [Online]. Available from: http://en.wikipedia.org/wiki/List_of_islands_of_Malaysia.

[31] M.A. Ashraf, I. Yusoff, M. Yusof, Y. Alias, Study of contaminant transport at an open-tipping waste disposal site, Environ. Sci. Poll. Res. 20 (2013) 4689–4710.

[32] S. Batool, S. Akib, M. Ahmad, K.S. Balkhair, M.A. Ashraf, Study of modern nano enhanced techniques for removal of dyes and metals, J. Nanomater. 2014 (2014) 1–20.

[33] Z.M. Darus, N.A. Hashim, S.N.A. Manan, M.A.A. Rahman, K.N.A. Maulud, O.A. Karim, N. Mastorakis, M. Poulos, V. Mladenov, Z. Bojkovic, Potential of wind energy in sustainable development of resort island in Malaysia: A case study of Pulau Perhentian (Perhentian Island), in: WSEAS International Conference. Proceedings of Mathematics and Computers in

Science and Engineering, World Scientific and Engineering Academy and Society (WSEAS), Corfu, 2008.
[34] Perhentian Island—Malaysia, in Turtle Bay Divers, 2013, [Online]. Available from: http://www.turtlebaydivers.com/DiveLocation.htm.
[35] R.G. Quayle, M. Changery, Estimates of coastal deepwater wave energy potential for the world, in: OCEANS 81, IEEE, Boston, MA, USA, 1981, pp. 903–907.
[36] D. Grenier, L.-A. Dessaint, O. Akhrif, Y. Bonnassieux, B. Le Pioufle, Experimental nonlinear torque control of a permanent-magnet synchronous motor using saliency, IEEE Trans. Ind. Elec. 44 (1997) 680–687.
[37] L. Jian, J. Liang, Y. Shi, G. Xu, A novel double-winding permanent magnet flux modulated machine for stand-alone wind power generation, Progr. Electromagn. Res. 142 (2013) 275–289.
[38] P.C. Krause, O. Wasynczuk, S.D. Sudhoff, S. Pekarek, Analysis of Electric Machinery and Drive Systems, Wiley, Hoboken, NJ, 2013.
[39] L. Barote, R. Weissbach, R. Teodorescu, C. Marinescu, M. Cirstea, Stand-alone wind system with vanadium redox battery energy storage, in: 11th International Conference on Optimization of Electrical and Electronic Equipment, 2008 (OPTIM 2008), IEEE, Braşov, Romania, 2008, pp. 407–412.

Appendix I

The battery bank rating calculation:

$$\text{Battery rating} = \frac{2.5\ \text{kW} \times 1\ \text{h}}{300\ \text{V} \times 0.6} = 13.89\ \text{A h}$$

Hence, 12-V, 14-Ahr battery rating is considered and consequently, 25 numbers of batteries are required to connect in series.

Appendix II

The Eq. (2) related to passive L–C filter design:

$$K = \left[\frac{k^2 - \frac{15}{4}k^4 + \frac{64}{5\pi}k^5 - \frac{5}{4}k^6}{1440}\right]^{1/2} \tag{24}$$

$$L_f = \frac{V_0}{I_0 f_{sw}} K \frac{V_{dclink}}{V_{0,av}} \left[1 + 4\pi^2 \left(\frac{f}{f_{sw}}\right)^2 K \frac{V_{dclink}}{V_{0,av}}\right]^{1/2} \tag{25}$$

$$C_f = \frac{V_{dclink}}{L_f f_{sw}^2 V_{0,av}} \tag{26}$$

where k—modulation index = 1; V_0—load voltage = 220 V; I_0—(load current) = 4.58 A; f—fundamental frequency = 50 Hz; f_{sw}—switching frequency = 2 kHz; $V_{0,av}$—total harmonic load voltage = 5% of V_0; L_f—inductance of filter; and C_f—capacitance of filter.

Appendix III

Table 1 Parameters of PMSG

Number of poles	4
Rated power	3 kW
Rated speed	241 rad/s
Per phase stator resistance (R)	0.4578 Ω
d-axis and q-axis stator inductance (L_d & L_q)	0.00334 H
Magnetic flux induced in the stator windings (ψ)	0.171 Wb
Rated torque	14.2 Nm

Table 2 Parameters of OWC

OWC chamber length (L_{ch})	1.5 m		
Water surface area inside the chamber (A_1)	1.4 m^2		
Turbine inlet area (A_2)	0.012 m^2		
Water depth (d)	WH (m)	WP (s)	d (m)
	0.98	4.9	16.47
	0.9	4.79	15.75
	0.88	4.79	15.73

Table 3 Parameters of Darrieus turbine

Swept area by balde (A)	0.012 m^2
Air density	1.22 Kg/m^3
Height of the rotor (H_t)	240 mm
Diameter of the rotor (D_t)	100 mm